**Electronic Supplementary Information**

# Tethered Molecular Redox Capacitor for Nanoconfinement-Assisted Electrochemical Signal Amplification

*Mijeong Kang,* ChaeWon Mun, Ho Sang Jung, Iris Baffour Ansah, Eunkyoung Kim, Haesik Yang, Gregory F. Payne, Dong-Ho Kim,* and Sung-Gyu Park**

Dr. M. Kang, C. Mun, Dr. H. S. Jung, I. B. Ansah, Dr. D.-H. Kim, Dr. S.-G. Park
Advanced Nano-Surface Department, Korea Institute of Materials Science (KIMS), Changwon, Gyeongnam 51508, South Korea
E-mail: mijeongkang@kims.re.kr, dhkim2@kims.re.kr, sgpark@kims.re.kr.

Dr. E. Kim, Prof. G. F. Payne
Institute for Bioscience and Biotechnology Research, University of Maryland, College Park, MD 20742, USA

Prof. H. Yang
Department of Chemistry, Pusan National University, Busan 46241, South Korea

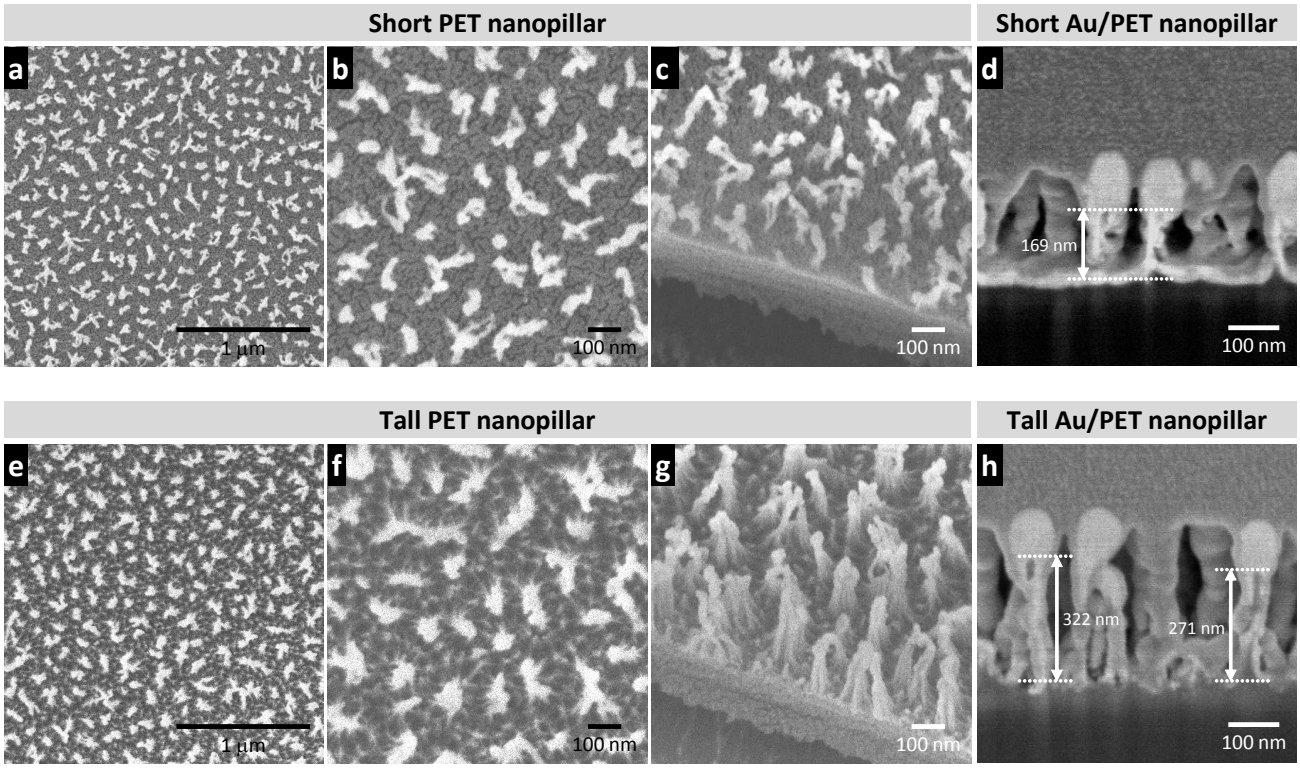


**Figure S1. Structure of nanopillars. (a-c)** Top (a,b) and tilted (c) view scanning electron microscopy (SEM) images of a short polyethylene terephthalate (PET) nanopillar substrate. **(d)** Cross-sectional SEM image of a short Au/PET nanopillar electrode. **(e-g)** Top (e,f) and tilted (g) view SEM images of a tall PET nanopillar substrate. **(h)** Cross-sectional SEM image of a tall Au/PET nanopillar electrode. In the cross-sectional images, the heights of PET nanopillars are indicated.

**Fabrication of Nanopillar Electrodes.** Au nanopillar electrodes were fabricated by Au deposition onto polymeric nanopillar substrates prepared via plasma treatment. In general, reactive ions in plasma can scissor and recombine the polymer chains; the modified chains often coalesce.[1-3] The resulting change in polymer morphology is dependent on the properties of both the plasma and the polymer substrate. By using two different plasma species, $CF_4$ and Ar, we controlled the surface morphology of polyethylene terephthalate (PET) substrates; $CF_4$ plasma treatment produced 167 ± 5 nm-high PET nanopillars, and the additional treatment with Ar plasma (after the same $CF_4$ plasma treatment) produced taller PET nanopillars (288 ± 32 nm high) (Figure S1). An Au thin film (150 nm thick) was deposited onto these PET

nanopillar substrates, resulting in a continuous Au film covering the substrate. In both short and tall nanopillar electrodes, a relatively thick Au film was formed on the nanopillar head, whereas the nanopillar sidewall and bottom surface were covered with a thin Au film. The variation in Au film thickness is attributed to the oblique direction (~45° angle) of Au deposition relative to the rotating PET nanopillar substrate in our sputtering system and the shadowing effect of neighboring PET nanopillars.[4, 5] As a control, a flat Au/PET electrode was fabricated by depositing Au onto the as-received PET substrate.

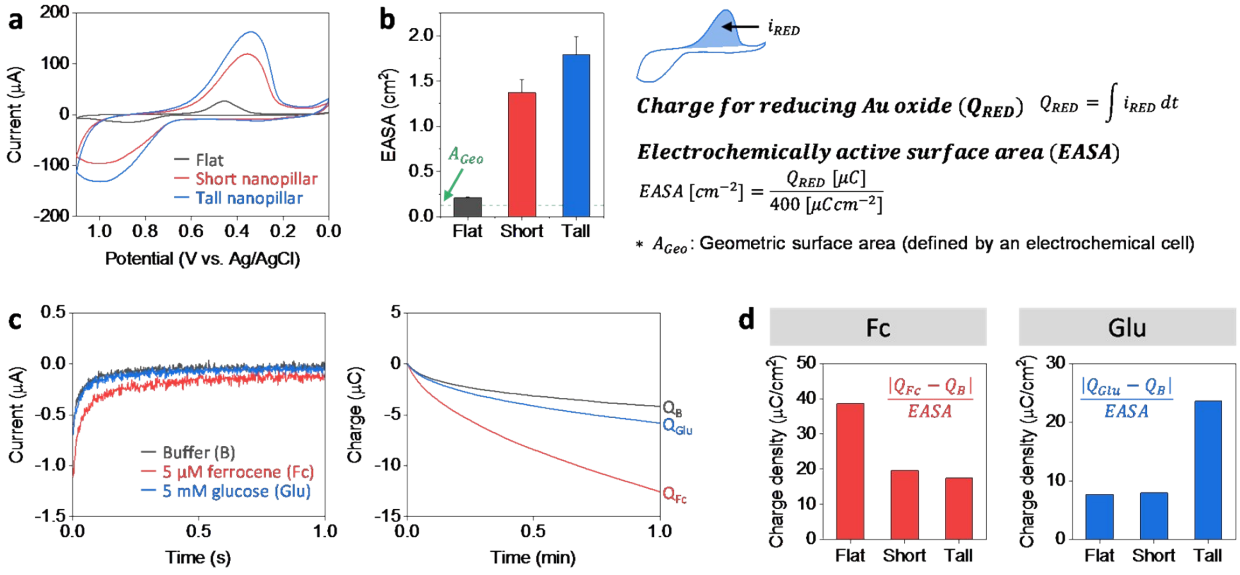


**Figure S2. Electrochemical characteristics of as-prepared nanopillar electrodes. (a)** Cyclic voltammograms for the Au oxidation and reduction of flat, short nanopillar, and tall nanopillar electrodes. **(b)** Electrochemically active surface areas (EASAs) of the electrodes, calculated from the charges for reducing Au oxide. **(c)** Amperometric curves obtained from a flat electrode (polarized at +0.5 V) (left) and the corresponding charge vs. time curves (right) for buffer (B), 5 μM ferrocene (Fc), and 5 mM glucose (Glu). $Q_B$, $Q_{Fc}$, and $Q_{Glu}$ denote the charge values at 1 min. **(d)** Faradaic charge densities for Fc oxidation (left) and Glu oxidation (right) at flat, short nanopillar, and tall nanopillar electrodes.

**Electrochemical Characteristics of As-Prepared Nanopillar Electrodes.** To calculate the electrochemically active surface areas (EASAs) of electrodes, cyclic voltammograms for the Au oxidation and reduction were obtained in a phosphate buffered solution (0.1 M, pH ~7.2) at a scan rate of 0.05 V/s (Figure S2a). EASA was calculated by dividing the charge for reducing Au oxide ($Q_{RED}$, integration of the cathodic current ($i_{RED}$, the current in the shaded region in Figure S2b) over time) by the charge per unit area required for that reduction, which is 400 μC/cm$^2$ for polycrystalline Au.[6] Geometric surface area ($A_{Geo}$) is the area of a Au electrode surface that is exposed to the solution, which is determined by the structure of our home-built electrochemical cell.

To investigate the behaviors of nanopillar electrodes to fast and slow electron transfer reactions, ferrocene (Fc) oxidation and glucose (Glu) oxidation, respectively, were conducted via amperometry (+0.5 V, 1 min) with flat, short nanopillar, and tall nanopillar electrodes. Representative amperometric curves (from a flat electrode) and the corresponding charge vs. time curves are shown in Figure S2c. The total charge values for 1 min reaction—$Q_B$, $Q_{Fc}$, and $Q_{Glu}$ obtained from buffer, Fc solution, and Glu solution, respectively—were used to calculate the density of faradaic charge, which is $|Q_{FC}-Q_B|$/EASA or $|Q_{Glu}-Q_B|$/EASA (Figure S2d). As generally expected for nanostructured electrodes,[7, 8] the nanopillar electrodes provided increased charge densities for glucose oxidation but decreased charge densities for Fc oxidation, compared with the flat electrode.

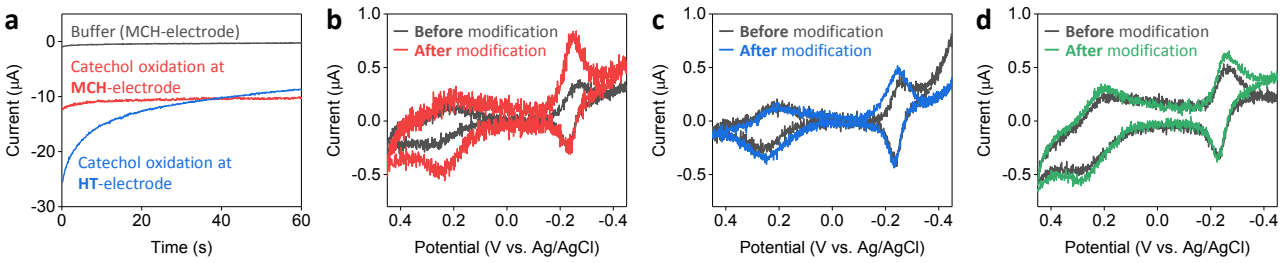


**e Surface modification**

| | Self-assembled monolayer on electrode surface | Electrode during the catechol graft reaction for 1 min |
|---|---|---|
| B | Mercaptohexanol (MCH) | Oxidized at +0.3 V |
| C | 1-hexanethiol (HT) | Oxidized at +0.3 V |
| D | MCH | No potential applied |

**Figure S3. Effect of surface modification on constructing redox-cycling system. (a)** Amperometric curves during the electrochemical catechol oxidation at the nanopillar electrodes modified with different self-assembled monolayer (mercaptohexanol (MCH) or 1-hexanethiol (HT)). **(b-d)** Background-subtracted cyclic voltammograms of 5 μM pyocyanin and 5 μM ferrocene measured at the nanopillar electrodes with different surface modification described in **e**. Significant signal amplification after surface modification is observed in b.

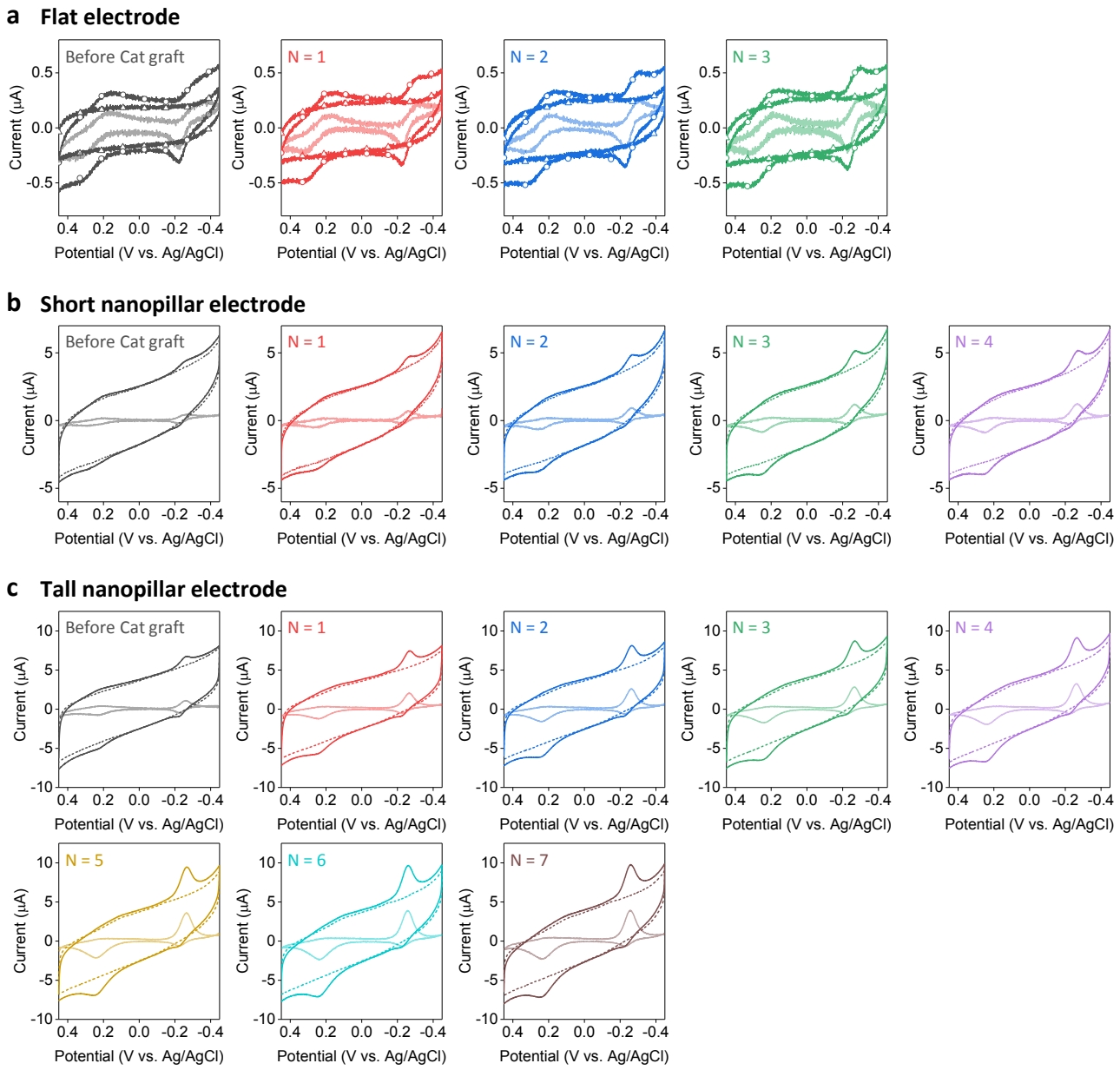


**Figure S4. Electrode-dependent redox-cycling reactions (original and background-subtracted cyclic voltammograms). (a-c)** *N*-times repetition of electrochemical catechol oxidation and the measurement of 5 μM pyocyanin and 5 μM ferrocene after each catechol oxidation for the flat (a), short nanopillar (b), and tall nanopillar (c) electrodes. Background cyclic voltammogram measured from a blank buffer (triangle in a; dark dashed line in b and c) was subtracted from the cyclic voltammogram of pyocyanin and ferrocene (circle in a; dark solid line in b and c) to obtain the background-subtracted cyclic voltammogram (light solid line in a, b, and c).

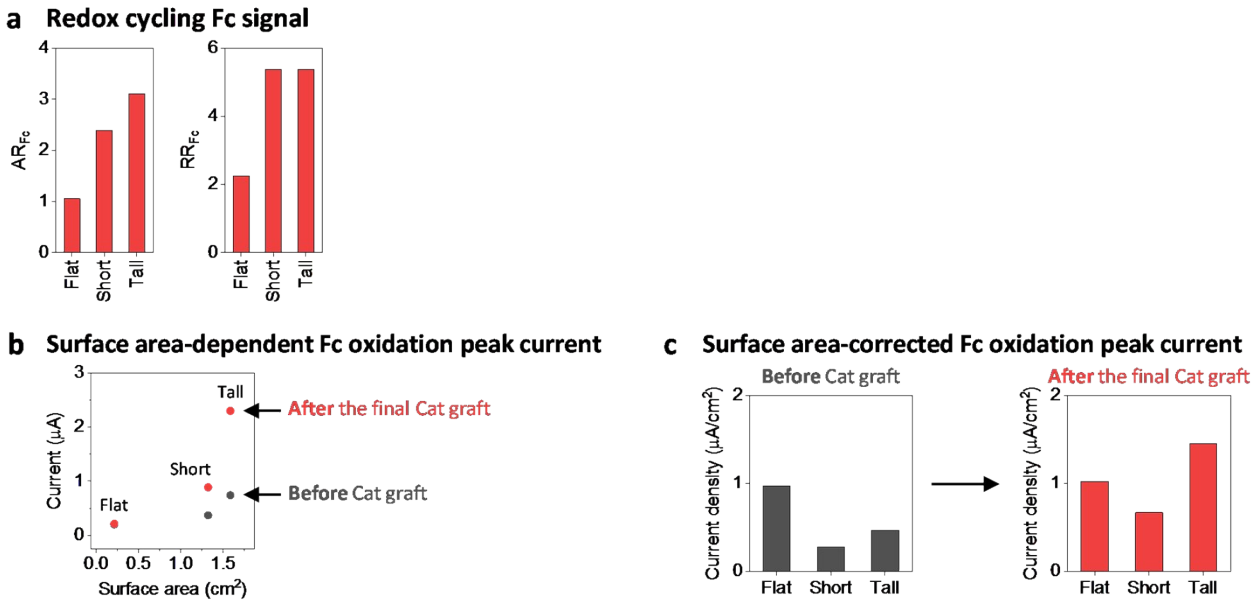


**Figure S5. Electrode-dependent redox-cycling reactions (ferrocene (Fc) signal in Figure 5). (a)** The amplification ratio (AR) and rectification ratio (RR) for the final Fc signals. **(b)** Fc oxidation peak currents before the catechol (Cat) graft (black) and after the final Cat graft (red) as a function of electrode surface area. **(c)** Current densities of the Fc oxidation peaks before the Cat graft and after the final Cat graft.

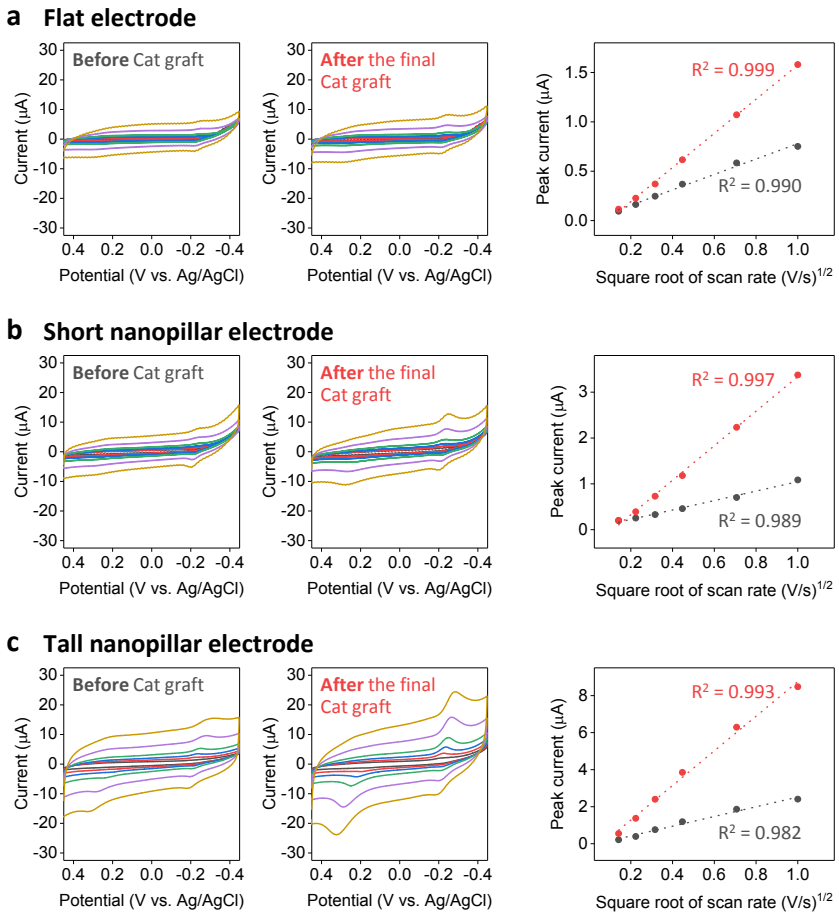


**Figure S6. Scan rate dependence of the electrochemical signal. (a-c)** Cyclic voltammograms of 5 μM pyocyanin and 5 μM ferrocene measured at flat (a), short nanopillar (b), and tall nanopillar (c) electrodes at scan rates of 20, 50, 100, 200, 500, 1000 mV/s before Cat graft (left) and after the final Cat graft (middle) with a corresponding plot of pyocyanin peak current vs. square root of scan rate (right). Linear relations between the peak current and square root of scan rate indicates that pyocyanin and ferrocene have fast electron-transfer kinetics and undergo diffusion-controlled electrochemical reactions.

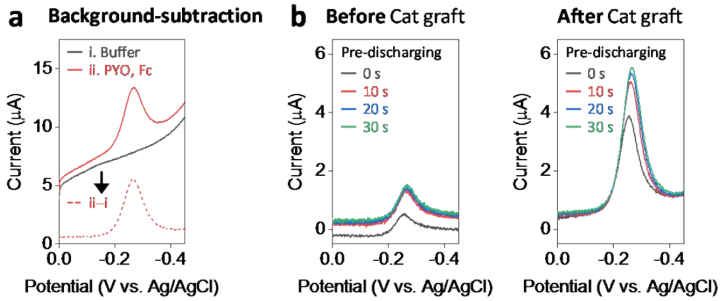


**Figure S7. Linear sweep voltammetry with catechol pre-discharging. (a)** Background-subtraction of linear sweep voltammogram for pyocyanin measurements: voltammogram of a blank buffer (i) is subtracted from that of 5 μM pyocyanin and 5 μM ferrocene (ii). **(b)** Effect of catechol/*o*-quinone (Cat) pre-discharging (at +0.4 V) time (0, 10, 20, 30 s): background-subtracted linear sweep voltammograms of 5 μM pyocyanin and 5 μM ferrocene measured at a Cat-grafted tall nanopillar electrode before (left) and after (right) Cat graft.

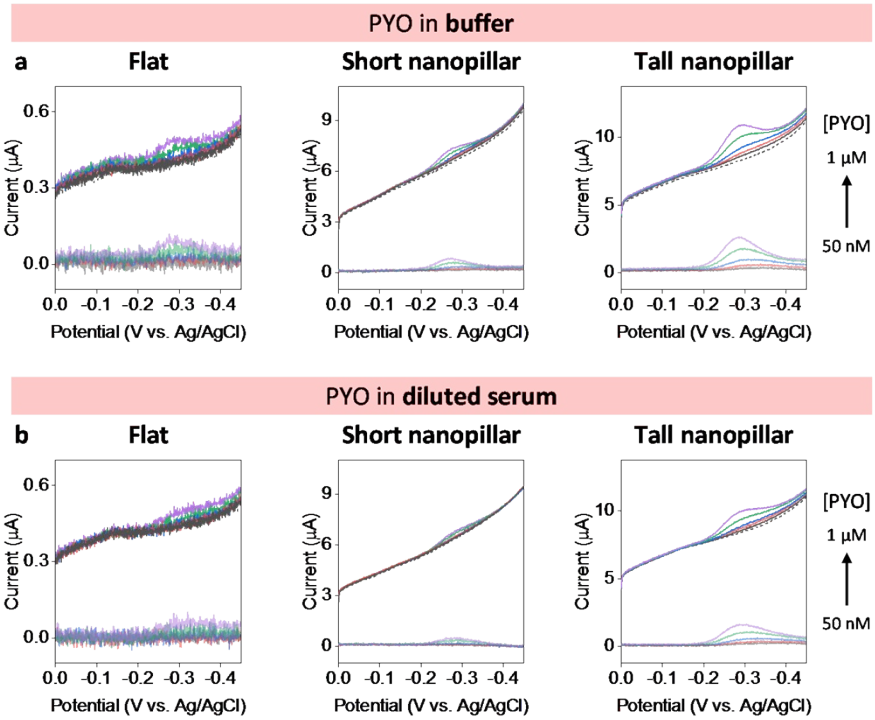


**Figure S8. Pyocyanin measurement using the catechol-grafted flat, short nanopillar, and tall nanopillar electrodes (original and background-subtracted linear sweep voltammograms). (a,b)** Original (dark solid line for the solutions of pyocyanin and ferrocene; dark dashed line for a blank solution) and background-subtracted (light solid line) linear sweep voltammograms (pyocyanin and ferrocene concentrations: 0.05, 0.1, 0.2, 0.5, 1 μM for each) recorded in buffered (a) and 100-times diluted serum (b) solutions.

**Table S1. Sensitivities of various electrochemical pyocyanin detection**

| Electrode material | Method | Buffer | Body fluid | | | Ref. |
|---|---|---|---|---|---|---|
| | | LOD (nM) | Specimen | Pretreatment | LOD (nM) | |
| Boron-doped diamond | DPV | 50 | Sputum | Extraction | 150 | 33 |
| Transparent carbon ultramicroelectrode array | SWV | 75 | - | - | - | 34 |
| Carbon ink | SWV | 3.33 | - | - | - | 35 |
| Screen-printed carbon | SWV | - | - | - | - | 36 |
| Screen-printed carbon | SWV | - | Cell culture | - | - | 37 |
| Carbon graphite ink | SWV | 150 | Serum | - | 169 | 38 |
| Carbon ink | SWV | 95 | - | - | - | 39 |
| Carbon felt | DPV | - | Cell culture | - | - | 40 |
| Au nanopillar | LSV | 16.3 | Serum | Dilution | 31.9 | This work |

DPV: differential pulsed voltammetry. SWV: square wave voltammetry. LOD: limit of detection

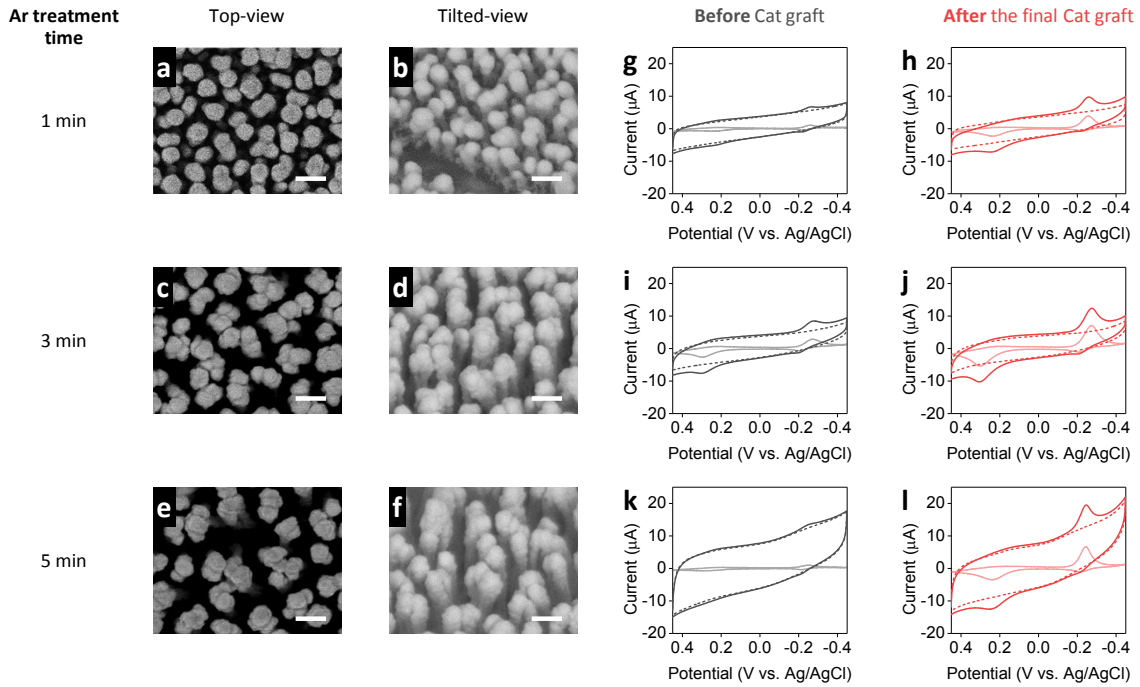


**Figure S9. Au nanopillar substrates fabricated with different Ar treatment time. (a-f)** Scanning electron microscopy images nanopillar electrodes fabricated with the Ar treatment for 1 min (a, b), 3 min (c, d), and 5 min (e, f) (scale bars: 200 nm). **(g-l)** Original cyclic voltammograms of a blank buffer (dark dashed line) and 5 μM pyocyanin and 5 μM ferrocene (dark solid line) and the corresponding background-subtracted cyclic voltammograms (light solid line) obtained before catechol/*o*-quinone (Cat) graft (g, i, k) and after the final Cat graft (h, j, l).

**Further Investigation of the Effect of Nanopillar Height.** The nanopillar height affects the electrochemical reaction by changing electrode morphology as well as electrode surface area, which in turn influences the electrochemical reaction rate and the sensitivity of electrochemical detection in a more complicated way than expected. To investigate this, we fabricated taller nanopillars than the "tall nanopillar". Since we added the Ar plasma treatment for 1 min to the fabrication process for the "tall nanopillar" (henceforth referred as nanopillar$_{1\ min}$), we prepared the taller nanopillars with the prolonged Ar plasma treatment to 3 and 5 min (nanopillar$_{3\ min}$ and nanopillar$_{5\ min}$, respectively) and modified their surface with the same method used for the nanopillar$_{1\ min}$. The SEM images of nanopillars (Figure S9a-f) show that with increasing the duration of Ar plasma treatment, the nanopillar length increases, but the

head-to-head distance increases as well because the nanopillars lean against one another; this "leaning effect" has been observed in literature.[9, 10] As the head-to-head separation increases, the interpillar space becomes more opened, likely reducing the nanoconfinement effect. Such contribution of leaning effect, however, would become negligible as the nanopillar length further increases. This is evinced by the electrochemical signal measured from nanopillar$_{3\ min}$ and nanopillar$_{5\ min}$ in comparison with the signal measured from nanopillar$_{1\ min}$. Figure S9i shows that the nanopillar$_{3\ min}$ before catechol/*o*-quinone (Cat) graft measures the significantly increased signals of pyocyanin (PYO) and ferrocene (Fc) relative to the small increment of background signal. This indicates the enhanced transport of PYO and Fc into the interpillar cavity (in other words, less confinement of the substances). The reduced signal amplification after Cat graft (Figure S9j) compared with the that observed from nanopillar$_{1\ min}$ (Figure S9g, h) is also ascribed to the reduced confinement of the substances and, therefore, the reduced frequency of their collision with Cat. In the case of nanopillar$_{5\ min}$, the background signal is significantly increased, indicating the significantly enlarged surface area (Figure S9k). PYO and Fc signals are not increased along with the background signal increment before Cat graft (Figure S9k), but substantially amplified after Cat graft (Figure S9l). This result implies the enhanced nanoconfinement makes the leaning effect less effective.

Although nanopillar$_{5\ min}$ provides the highest signal amplification, it does not guarantee the highest detection sensitivity; the limits of detection (LODs) calculated by the general 3$\sigma$ method are 16.3 nM for nanopillar$_{1\ min}$, 16.6 nM for nanopillar$_{3\ min}$, and 30.8 nM for nanopillar$_{3\ min}$. Increased LOD obtained from the nanopillar$_{5\ min}$ is attributed to the increased background signal and, subsequently, increased 3$\sigma$ value.

## References


1. R. Di Mundo, M. Troia, F. Palumbo, M. Trotta and R. d'Agostino, *Plasma Process. Polym.*, 2012, **9**, 947-954.
2. J. Yun, W. Wang, S. M. Kim, T.-S. Bae, S. Lee, D. Kim, G.-H. Lee, H.-S. Lee and M. Song, *Energ Environ. Sci.*, 2015, **8**, 932-940.
3. S. Lee, E. Byeon, S. Jung and D. G. Kim, *Sci. Rep.*, 2018, **8**, 14063.
4. S.-G. Park, C. Mun, X. Xiao, A. Braun, S. Kim, V. Giannini, S. A. Maier and D.-H. Kim, *Adv. Funct. Mater.*, 2017, **27**, 1703376.

5. X. Wang, S. G. Park, J. Ko, X. Xiao, V. Giannini, S. A. Maier, D. H. Kim and J. Choo, *Small*, 2018, **14**, 1801623.
6. J. C. Hoogvliet, M. Dijksma, B. Kamp and W. P. van Bennekom, *Anal. Chem.*, 2000, **72**, 2016-2021.
7. R. Szamocki, S. Reculusa, S. Ravaine, P. N. Bartlett, A. Kuhn and R. Hempelmann, *Angew. Chem. Int. Ed.*, 2006, **45**, 1317-1321.
8. K. Sanger, O. Durucan, K. Wu, A. H. Thilsted, A. Heiskanen, T. Rindzevicius, M. S. Schmidt, K. Zor and A. Boisen, *ACS Sens.*, 2017, **2**, 1869-1875.
9. M. K. Choi, H. Yoon, K. Lee and K. Shin, *Langmuir*, 2011, **27**, 2132-2137.
10. V. Anandan, Y. L. Rao and G. G. Zhang, *Int J Nanomed*, 2006, **1**, 73-79.